Nano-Micro Lett. (2017) 9:34
DOI 10.1007/s40820-017-0127-7

ARTICLE

Formation of $NiFe_2O_4$/Expanded Graphite Nanocomposites with Superior Lithium Storage Properties

Yinglin Xiao[1,2] · Jiantao Zai[2] · Bingbing Tian[1,3] · Xuefeng Qian[2]

Received: 9 November 2016 / Accepted: 26 December 2016 / Published online: 21 February 2017

Highlights

- A $NiFe_2O_4$/expanded graphite ($NiFe_2O_4$/EG) nanocomposite was synthesized via a simple grinding and mixing process followed by annealing at a high temperature. The obtained $NiFe_2O_4$/EG nanocomposite showed superior lithium storage properties, with a capacity of 601 mAh g^{-1} at a current density of 1 A g^{-1} after 800 cycles.
- The hybrid$NiFe_2O_4$/EG nanostructure could efficiently improve the electrical conductivity and maintain structure stability, and its disintegration was delayed during discharge–charge processes, which led to a good cycling performance.

Abstract A $NiFe_2O_4$/expanded graphite ($NiFe_2O_4$/EG) nanocomposite was prepared via a simple and inexpensive synthesis method. Its lithium storage properties were studied with the goal of applying it as an anode in a lithium-ion battery. The obtained nanocomposite exhibited a good cycle performance, with a capacity of 601 mAh g^{-1} at a current of 1 A g^{-1} after 800 cycles. This good performance may be attributed to the enhanced electrical conductivity and layered structure of the EG. Its high mechanical strength could postpone the disintegration of the nanocomposite structure, efficiently accommodate volume changes in the $NiFe_2O_4$-based anodes, and alleviate aggregation of $NiFe_2O_4$ nanoparticles.

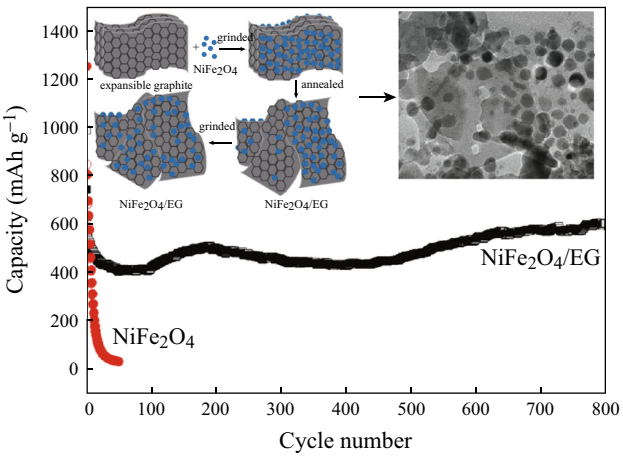

✉ Bingbing Tian
chmt@nus.edu.sg

✉ Xuefeng Qian
xfqian@sjtu.edu.cn

[1] SZU-NUS Collaborative Innovation Center for Optoelectronic Science and Technology, Key Laboratory of Optoelectronic Devices and Systems of Ministry of Education and Guangdong Province, College of Optoelectronic Engineering, Shenzhen University, Shenzhen 518060, People's Republic of China

[2] School of Chemistry and Chemical Engineering, State Key Laboratory of Metal Matrix Composites, Shanghai Jiao Tong University, Shanghai 200240, People's Republic of China

[3] Department of Chemistry, National University of Singapore, 3 Science Drive 3, Singapore 117543, Singapore

Keywords $NiFe_2O_4$ · Expanded graphite · Anode materials · Lithium-ion batteries

1 Introduction

To meet the demands of high-energy storage for practical applications in electric vehicles (EVs) and hybrid electric vehicles (HEVs), much attention has been paid to lithium-ion batteries (LIBs) because of their distinct advantages, e.g., their large specific capacity, high energy density, long cycle life, and environmental friendliness [1–3]. Today, there is a great demand to design and develop novel and high-performance electrode materials to achieve LIBs with higher energy density, longer cycle life, improved safety, and lower cost. However, it is still urgency to improve the reversible charge capacity of anode materials in commercial LIBs, i.e., graphite [4, 5]. Among various anode materials with higher specific capacities than that of the material used in commercial batteries, ternary compounds (e.g., $CuFe_2O_4$ [6, 7], $ZnFe_2O_4$ [8, 9], $CoFe_2O_4$ [10–12], Zn_2SnO_4 [9, 13], $ZnMn_2O_4$ [14–17]) have been considered promising candidates because of their high theoretical capacities, low cost, and safety [9]. Nevertheless, their poor electrical conductivities and huge volume changes during continuous charge–discharge processes would lead to electrode pulverization. Rapid disintegration of these electrode materials caused by induced mechanical stress is responsible for a decrease in the capacity upon cycling and further hinders their practical applications [18, 19]. Expanded graphite (EG) possesses many advantageous properties, including fewer functional groups, better conductivity, higher mechanical strength [20], and lower cost [21]. A layered $NiFe_2O_4$/EG composite structure can be fabricated by incorporating nanostructured $NiFe_2O_4$ material with EG. This provides outstanding electron conductivity [22–25] and an ideal solution to the aforementioned inherent drawbacks of ternary compounds. However, to the best of our knowledge, there have been few reports on the construction of nanostructured material/EG composites with superior lithium storage properties because it is a challenge to homogenously disperse nanostructured materials into EG nanosheets.

In this work, a $NiFe_2O_4$/EG nanocomposite was easily fabricated via a grinding and mixing process, followed by annealing at a high temperature. This $NiFe_2O_4$/EG nanocomposite showed superior lithium storage properties, with a capacity of 601 mAh g^{-1} at a current density of 1 A g^{-1} after 800 cycles. In general, the combination of several structural features of the $NiFe_2O_4$/EG nanocomposite may contribute to the enhanced capacity and cycling performance. First, the layered structure of the $NiFe_2O_4$/EG nanocomposite can alleviate agglomeration of materials and improve the cycling performance. Second, the higher mechanical strength of EG can postpone disintegration of the nanocomposite structure. Third, EG can provide an enhanced conductivity performance, which is critical for the lithium storage performance. Fourth, EG has a high reversible capacity and good cycling performance, which can assist in enhancing the capacity and cycling performance of $NiFe_2O_4$/EG nanocomposite.

2 Experimental

2.1 Synthesis of $NiFe_2O_4$ and $NiFe_2O_4$/EG Nanocomposites

$NiFe_2O_4$ was synthesized using the procedure reported in a previous paper [26]. Typically, 1 mmol of nickel chloride hexahydrate ($NiCl_2{\cdot}6H_2O$), 2 mmol of ferric chloride hexahydrate ($FeCl_3{\cdot}6H_2O$), and 3 mL of ammonia were dissolved in 37 mL of alcohol. The mixture was sonicated for 30 min, transferred to a Teflon-lined autoclave, and then maintained at 180 °C for 12 h. The final product was separated by centrifugation and dried at 60 °C.

The $NiFe_2O_4$/EG nanocomposite was synthesized using the following procedure: 0.5 g of $NiFe_2O_4$, 0.2 g of expandable graphite, and 5 mL of alcohol were mixed and ground until the alcohol was completely volatilized. After that, the mixture was annealed at 1000 °C for 5 min in an Ar atmosphere, and the final product was ground and used as the active material for lithium-ion batteries.

2.2 Characterizations

The crystal structures of the powder samples were characterized using X-ray diffraction (XRD, Shimadzu XRD-6000, CuKα, 40 kV, 30 mA, $20° \leq 2\theta \leq 70°$). A thermogravimetric (TG) analysis was performed on a PerkinElmer 7 instrument to determine the weight ratio of EG to $NiFe_2O_4$. The morphology of each sample was studied using a transmission electron microscopy (TEM) system (JEOL, JEM-2100).

2.3 Electrochemical Testing

The working electrodes were fabricated from a slurry containing 80% active material, 10% polymer binder (polyvinylidene difluoride, PVDF), and 10% acetylene black on a copper foil using the procedure outlined in previous work [27] and dried in a vacuum oven at 80 °C for 12 h. The electrochemical performances were determined using a LAND battery tester (CT2001A model, Wuhan Jinnuo Electronics, Ltd.) between 0.01 and 3 V versus Li^+/Li. All of the tests were performed at room temperature, with an electrolyte composed of 1 mol L^{-1} of

$LiPF_6$ in a mixed solvent of ethylene carbonate (EC)/diethylene carbonate (DEC) (1:1 vol%) and a Li cathode placed in the cell. Cyclic voltammetry measurements were performed using a CHI 660C potentiostat between 0.01 and 3 V at a scan speed of 0.5 mV s^{-1}. A frequency range of 10 kHz to 0.1 Hz was used for electrochemical impedance spectroscopy (EIS) at an open-circuit potential with an alternating spectrum (AC) perturbation of 10 mV on a Zennium electrochemistry workstation.

3 Results and Discussion

The synthesis procedure is schematically depicted in Fig. 1. In the first step, $NiFe_2O_4$ is homogenously dispersed onto the surface of the EG after the grinding process. After the calcination process, a mixture of thermal EG nanosheets and $NiFe_2O_4$ is obtained. Finally, $NiFe_2O_4$ is homogenously dispersed onto the surface of the EG nanosheets during the grinding process, producing the desired $NiFe_2O_4$/EG nanocomposites.

The XRD pattern of $NiFe_2O_4$ in Fig. 2a shows that all of the diffraction peaks can be readily indexed to cubic $NiFe_2O_4$ (JCPDS card no. 227, space group: Fd-3 m, $a = 8.33790$ Å). One additional diffraction peak located at approximately 26.2° in the XRD pattern of $NiFe_2O_4$/EG suggests the presence of EG. No other additional peaks are observed in the XRD patterns, suggesting high purity of the obtained products. The weight ratio of EG in the $NiFe_2O_4$/EG nanocomposite was evaluated using TGA in air (Fig. 2b). Assuming that the final residue was $NiFe_2O_4$, the lost weight of $NiFe_2O_4$/EG may correspond to the oxidation of EG to CO_2. Based on the lost weight values of the $NiFe_2O_4$ and $NiFe_2O_4$/EG nanocomposites, the weight percentage of EG in the $NiFe_2O_4$/EG was approximately 14%.

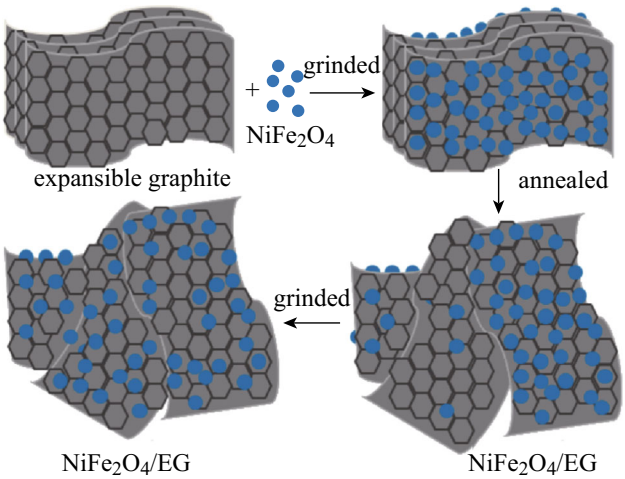

Fig. 1 Schematic illustration of possible formation mechanism of $NiFe_2O_4$/EG nanocomposite

The morphologies and structures of the as-prepared $NiFe_2O_4$ and $NiFe_2O_4$/EG nanocomposites were studied using TEM. It was found that the size of the as-prepared $NiFe_2O_4$ was approximately 20 nm (Fig. 3a); $NiFe_2O_4$ was homogenously dispersed into the paper-like EG nanosheets in the $NiFe_2O_4$/EG nanocomposite (Fig. 3b). Furthermore, the structural characteristics of a typical $NiFe_2O_4$ nanoparticle with visible lattice fringes were observed in the HRTEM image (Fig. 3c). Inter-planar distances of 0.294 and 0.240 nm were measured, which were consistent with the (220) and (222) crystal planes of the cubic $NiFe_2O_4$ phase, respectively, confirming the crystalline structure of the obtained $NiFe_2O_4$.

The lithium storage properties of the $NiFe_2O_4$/EG nanocomposite as an anode material for LIBs were studied using CV between 0 and 3.0 V vs. Li/Li^+ at a scan rate of 0.0005 V s^{-1} (Fig. 4). In the first CV cycle, the broad cathodic peak located at approximately 0.40 V could be attributed to the reduction reactions of Ni^{2+} to Ni^0 and/or Fe^{3+} to Fe^0. It is known that the first discharge plateaus of NiO and Fe_2O_3 are usually located at 0.26 and 0.55, respectively [28, 29]. Thus, the reduction peaks of $NiFe_2O_4$ could have overlapped to form a broad cathodic peak at 0.45 under our experimental conditions. This cathodic peak shifted to ~0.80 V in the second and subsequent cycles, corresponding to a lower polarization of the electrodes induced by the first lithiation–delithiation process. This process can be expressed by the following reaction:

$$NiFe_2O_4 + 8Li^+ + 8e^- \rightarrow Ni + 2Fe + 4Li_2O \quad (1)$$

The anodic peak located at 1.75 V in the first CV cycle may correspond to the oxidation of metallic Fe and Ni, and this anodic peak shifts to 1.90 V in subsequent cycles because of the polarization of the electrodes [3, 30]. This process can be expressed by the following reactions:

$$Ni + Li_2O \rightarrow NiO + 2Li^+ + 2e^- \quad (2)$$

$$2Fe + 3Li_2O \rightarrow Fe_2O_3 + 6Li^+ + 6e^- \quad (3)$$

The reversible cathodic and anodic peaks located at approximately 0.80 and 1.90 V, respectively, in the second and subsequent cycles indicate a reversible oxidation–reduction reaction in the charge–discharge processes. To summarize, the reaction should be as follows:

$$Ni + 2Fe + 4Li_2O \leftrightarrow NiO + Fe_2O_3 + 8Li^+ + 8e^- \quad (4)$$

Moreover, the observed small cathodic peaks at 0.1 V and anodic peaks located at 0.25 V may correspond to the reversible polymerization/oligomerization of carbonates and alkyl carbonates (the main components of the solid-

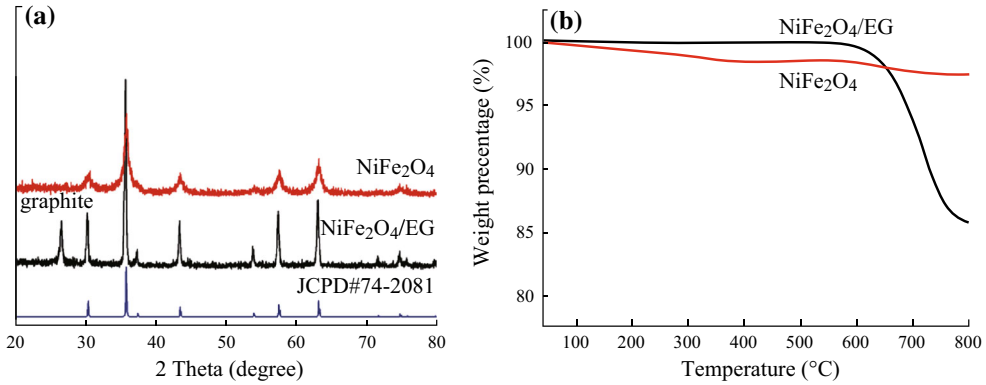

Fig. 2 **a** XRD patterns and **b** TGA results for $NiFe_2O_4$ and $NiFe_2O_4$/EG

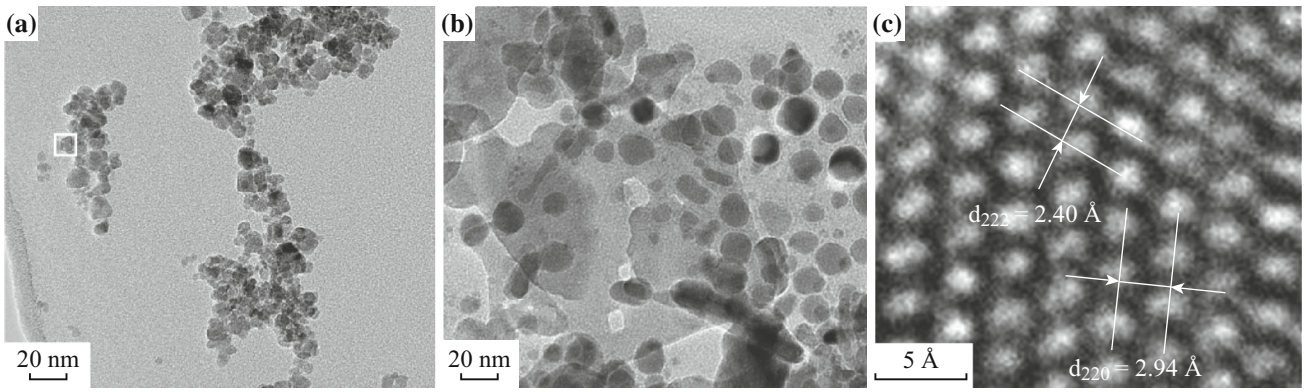

Fig. 3 TEM images of **a** $NiFe_2O_4$ and **b** $NiFe_2O_4$/EG and HRTEM image of $NiFe_2O_4$

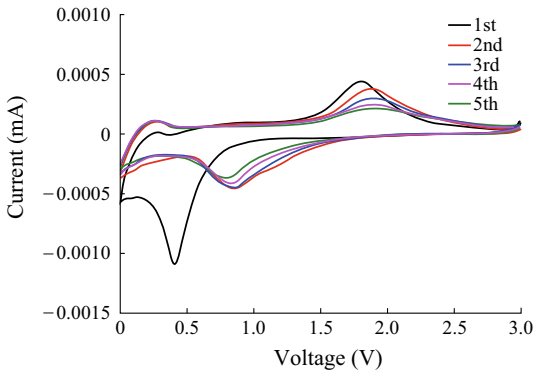

Fig. 4 Cyclic voltammograms of $NiFe_2O_4$/EG nanocomposites for first five cycles between 3.00 and 0.01 V vs. Li, with scan rate of 0.5 mV s^{-1}

state electrolyte interface), which would further lead to a reversible polymeric/gel film on the nanocomposite [31, 32].

The discharge–charge voltage profiles of the $NiFe_2O_4$/EG nanocomposite at a current density of 0.1 A g^{-1} are shown in Fig. 5a. The electrode based on $NiFe_2O_4$/EG had only one discharge platform, located at 0.75 V, which is attributed to the reduction reaction of $NiFe_2O_4$ with lithium during the first discharge process and is also associated with the formation of a solid-state electrolyte interface (SEI) [4]. The plateau increased to ~1.0 V in the subsequent cycles, in agreement with the galvanostatic discharge–charge data [33]. After the 10th cycle, the plateau at approximately 1.0 V had evolved into a slope, which may have been caused by Li^+ trapping in the electrode during cycling [34]. The fact that the specific capacity was greater than 0.75 V in the first cycle and greater than 1.0 V in the subsequent cycles could be ascribed to the faradic capacitance on the surface or edge site of the EG. A similar phenomenon can be found in graphene nanosheets [35]. The fact that the capacity was less than 0.75 V in the first cycle and less than 1.0 V in subsequent cycles was mainly associated with the conversion–deconversion process of the binary oxide and the formation of the SEI layer [36]. The excellent mechanical property of EG can postpone the disintegration of the nanocomposite structure during the discharge–charge processes and leads to a good cycle performance [37, 38].

Figure 5b shows the cyclic performances of $NiFe_2O_4$ and $NiFe_2O_4$/EG at a current density of 1 A g^{-1}. A discharge capacity of 986 mAh g^{-1} and a charge capacity of 741 mAh g^{-1} in the first cycle were observed

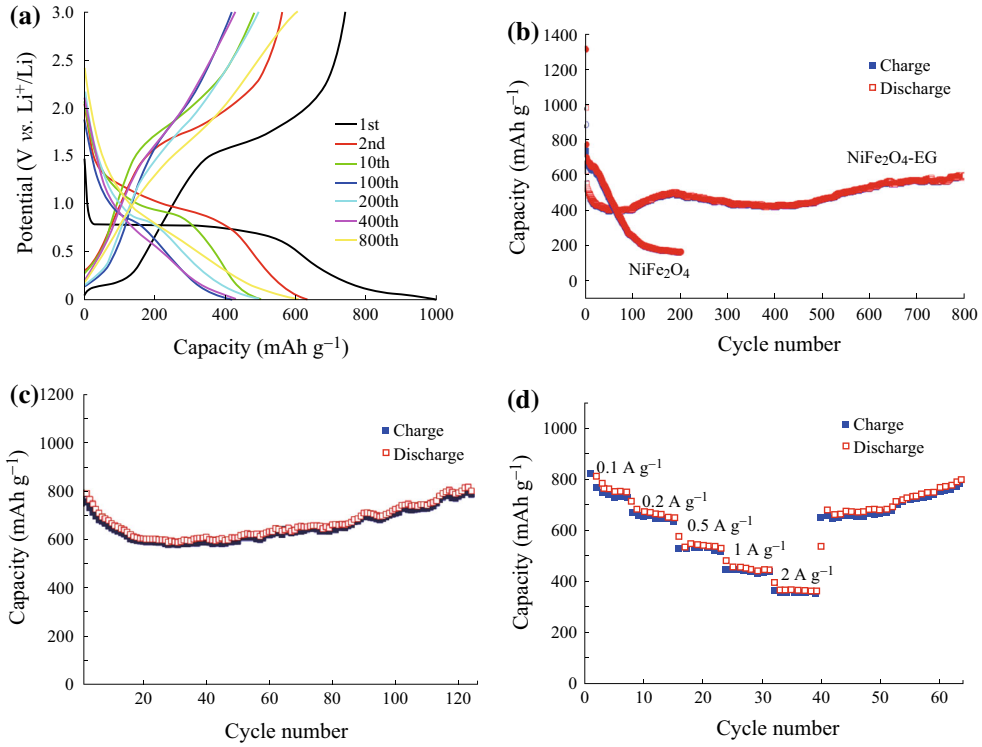

Fig. 5 **a** Charge–discharge curves of $NiFe_2O_4$/EG at 0.1 A g^{-1}, **b** cycling performances of $NiFe_2O_4$ and $NiFe_2O_4$/EG at current density of 1 A g^{-1}, **c** cycling performance of $NiFe_2O_4$/EG at current density of 0.1 A g^{-1}, and **d** rate capability of $NiFe_2O_4$/EG

on the $NiFe_2O_4$/EG electrode. The large initial irreversible discharge capacity could be attributed to the formation of the SEI. The capacities continued to decrease until the 50th cycle. This capacity decrease was partially ascribed to the decomposition of the electrolyte [39], along with the incompletely reversible reaction of the $NiFe_2O_4$/EG nanocomposite. It is interesting to note that after the 100th cycle, the reversible capacities significantly increased with the further activation of $NiFe_2O_4$, which was also observed in earlier work [40]. Furthermore, the reversible capacities of the $NiFe_2O_4$/EG continued to increase from 443 mAh g^{-1} in the 450th cycle to 601 mAh g^{-1} in the 800th cycle. These increasing capacities can be attributed to the reversible polymeric/gel film on the nanocomposite. A similar phenomenon has been observed in other transition metal oxides [37, 41]. The cyclic stability of the $NiFe_2O_4$/EG nanocomposite electrode was better than those reported in previous papers [42, 43]. The results indicated that the excellent mechanical properties of the EG contributed to the cyclic stability of the obtained $NiFe_2O_4$/EG composite.

The cycling performance of the $NiFe_2O_4$/EG at a current density of 0.1 A g^{-1} up to 120 cycles is shown in Fig. 5c. The initial discharge capacity (1182 mAh g^{-1}) was much higher than the charge capacity (790 mAh g^{-1}), with a high irreversible capacity (a Coulombic efficiency of 66.8%) related to the formation of an SEI layer and a non-fully reversible conversion–deconversion process in the first lithiation–delithiation cycle. In subsequent cycles, the discharge and charge capacities were almost equal, with a Coulombic efficiency of ~100%, which indicated excellent electrochemical reversibility. The capacity decreased slightly from the second to 20th cycle because of the non-fully reversible conversion–deconversion process and then slowly increased from the 21st to 120th cycle because of the reactivation of the $NiFe_2O_4$. The $NiFe_2O_4$/EG electrode material was collected after the 120th discharge–charge process and further analyzed using TEM (Fig. 6). The TEM image showed that the EG in the $NiFe_2O_4$-EG still had a layered structure and there was no agglomeration of $NiFe_2O_4$ nanoparticles, which was responsible for the good stability of the electrode. To further evaluate the stability of the $NiFe_2O_4$/EG nanocomposite, the rate capability was investigated at different rates from 0.1 to 2 A g^{-1} (Fig. 5d). The electrode had charge capacities of 824, 667, 529, and 445 mAh g^{-1} at current densities of 0.1, 0.2, 0.5, and 1.0 A g^{-1}, respectively. Furthermore, at a current density of 2.0 A g^{-1}, the $NiFe_2O_4$/EG electrode had a stable charge capacity of 361 mAh g^{-1}, indicating that the obtained $NiFe_2O_4$/EG nanocomposite exhibited a remarkable high lithium storage capacity at a high rate.

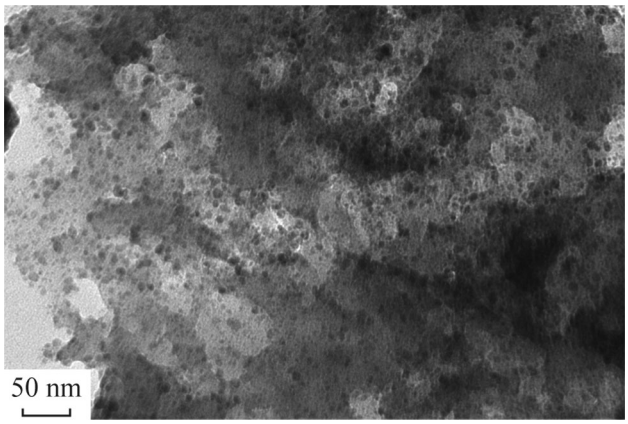

Fig. 6 TEM images of $NiFe_2O_4$/EG nanocomposite after 120 discharge–charge processes

To further investigate the effects of the EG in the $NiFe_2O_4$/EG nanocomposite, the conductivities of $NiFe_2O_4$ and $NiFe_2O_4$/EG after five discharge–charge cycles were evaluated using EIS measurements (Fig. 7). As widely discussed in EIS studies of intercalation–deintercalation-type materials, the semicircle in the medium-frequency region is assigned to the charge-transfer impedance, which is related to the electrochemical reaction between the electrolyte and electrode [6, 44]. In the plots for $NiFe_2O_4$ and its nanocomposite, the semicircle for the $NiFe_2O_4$/EG nanocomposite is smaller than that of $NiFe_2O_4$, indicating that the EG could facilitate the electron transfer between the electrolyte and $NiFe_2O_4$ and further improve the rate capability [45].

Based on the above discussion, the advantage of the $NiFe_2O_4$/EG nanocomposite involves its unique structural and electrochemical nature. First, the layered structure of the $NiFe_2O_4$/EG nanocomposite can alleviate the agglomeration of materials and improve the cycling performance. Second, EG has fewer functional groups and excellent mechanical properties, which can maintain the structure stability and postpone the disintegration of the nanocomposite structure during the discharge–charge processes, leading to a good cycle performance. Third, the high electrical conductivity of EG can increase the conductivity of the electrodes, ensuring fast electron transportation. Finally, EG has a high reversible capacity and good cycle performance, which is conducive to enhancing the capacity and cycling performance [46].

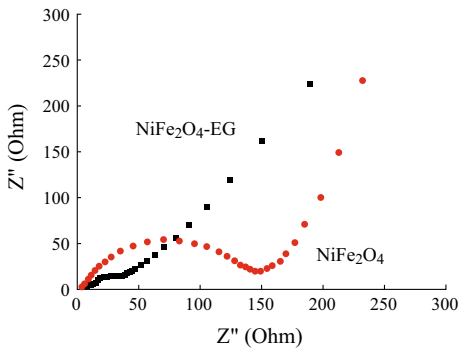

Fig. 7 Nyquist plots of $NiFe_2O_4$ and $NiFe_2O_4$/EG at 0.08 V vs. Li after five cycles

4 Conclusions

We developed a simple method for the direct homogeneous dispersion of $NiFe_2O_4$ nanoparticles onto EG nanosheets for use as a superior anode material for lithium-ion batteries. This hybrid nanostructure showed improved electrical conductivity, maintained structure stability, and exhibited delayed disintegration during the discharge–charge processes, which led to a good cycle performance. As a result, the fabricated $NiFe_2O_4$/EG composite demonstrated a high reversible capacity of 601 mAh g^{-1} over 800 cycles at a current density of 1 A g^{-1}. Our synthesis approach could easily be extended to combine other ternary compounds (MFe_2O_4, MCo_2O_4, MMn_2O_4, etc.) with EG, offering promising routes for the low-cost mass production of advanced electrode materials for the next generation of LIBs.

Acknowledgements The authors acknowledge the support from the National Basic Research Program of China (2014CB239702), National Natural Science Foundation of China (Grant Nos. 21371121, 21506126 and 51502174) and Shenzhen Science and Technology Research Foundation (Grant Nos. JCYJ20150324141711645,JCYJ20150324141711616 and JCYJ20150626090504916), and China Postdoctoral Science Foundation (2015 M582401 and 2015 M572349).

References

1. D. Wu, Z. Guo, X. Yin, Q. Pang, B. Tu, L. Zhang, Y.G. Wang, Q. Li, Metal-organic frameworks as cathode materials for Li-O_2 batteries. Adv. Mater. **26**(20), 3258–3262 (2014). doi:10.1002/adma.201305492
2. G. Xu, B. Ding, J. Pan, P. Nie, L. Shen, X. Zhang, High performance lithium-sulfur batteries: advances and challenges. J. Mater. Chem. A **2**(32), 12662–12676 (2014). doi:10.1039/C4TA02097A
3. H. Liao, H. Ding, B. Li, X. Ai, C. Wang, Covalent-organic frameworks: potential host materials for sulfur impregnation in

lithium–sulfur batteries. J. Mater. Chem. A **2**(23), 8854–8858 (2014). doi:10.1039/c4ta00523f
4. Y. Sun, J. Zhang, T. Huang, Z. Liu, A. Yu, Fe_2O_3 CNTs composites as anode materials for lithium-ion batteries. Int. J. Electrochem. Sci. **8**(2), 2919–2931 (2013)
5. Y. Liu, X. Zhao, F. Li, D. Xia, Facile synthesis of MnO/C anode materials for lithium-ion batteries. Electrochim. Acta **56**(18), 6448–6452 (2011). doi:10.1016/j.electacta.2011.04.133
6. S. Peng, L. Li, M. Srinivasan, Electrospun $CuFe_2O_4$ nanotubes as anodes for high-performance lithium-ion batteries. J. Energy Chem. **23**(3), 301–307 (2014). doi:10.1016/S2095-4956(14)60151-0
7. L. Luo, R. Cui, H. Qiao, K. Chen, Y. Fei, D. Li, Z. Pang, K. Liu, Q. Wei, High lithium electroactivity of electrospun $CuFe_2O_4$ nanofibers as anode material for lithium-ion batteries. Electrochim. Acta **144**, 85–91 (2014). doi:10.1016/j.electacta.2014.08.048
8. J. Shi, X. Zhou, Y. Liu, Q. Su, J. Zhang, G. Du, One-pot solvothermal synthesis of $ZnFe_2O_4$ nanospheres/graphene composites with improved lithium-storage performance. Mater. Res. Bull. **65**, 204–209 (2015). doi:10.1016/j.materresbull.2015.01.057
9. Y. Dong, Y. Xia, Y.S. Chui, C. Cao, J.A. Zapien, Self-assembled three-dimensional mesoporous $ZnFe_2O_4$-graphene composites for lithium ion batteries with significantly enhanced rate capability and cycling stability. J. Power Sources **275**, 769–776 (2015). doi:10.1016/j.jpowsour.2014.11.005
10. X. Liu, N. Wu, C. Cui, P. Zhou, Y. Sun, Enhanced rate capability and cycling stability of core/shell structured $CoFe_2O_4$/onion-like C nanocapsules for lithium-ion battery anodes. J. Alloys Compd. **644**, 59–65 (2015). doi:10.1016/j.jallcom.2015.04.097
11. X. Zhang, Y. Xie, Y. Sun, Q. Zhang, Q. Zhu, D. Hou, J. Guo, Self-template synthesis of $CoFe_2O_4$ nanotubes for high-performance lithium storage. RSC Adv. **5**(38), 29837–29841 (2015). doi:10.1039/c5ra00428d
12. J. Guo, X. Zhang, Y. Sun, X. Zhang, Mesoporous $CoFe_2O_4$ octahedra with high-capacity and long-life lithium storage properties. RSC Adv. **6**(1), 18–22 (2016). doi:10.1039/c5ra21311h
13. S. Hu, Y. Song, S. Yuan, H. Liu, Q. Xu, Y. Wang, C.-X. Wang, Y.-Y. Xia, A hierarchical structure of carbon-coated Li_3VO_4 nanoparticles embedded in expanded graphite for high performance lithium ion battery. J. Power Sour. **303**, 333–339 (2016). doi:10.1016/j.jpowsour.2015.11.015
14. J. Guo, H. Zhu, Y. Sun, L. Tang, X. Zhang, Flexible foams of graphene entrapped SnO_2-Co_3O_4 nanocubes with remarkably large and fast lithium storage. J. Mater. Chem. A **4**, 16101–16107 (2016). doi:10.1039/C6TA06626G
15. T. Jiang, X. Tian, H. Gu, H. Zhu, Y. Zhou, Zn_2SnO_4@C core–shell nanorods with enhanced anodic performance for lithium-ion batteries. J. Alloys Compd. **639**, 239–243 (2015). doi:10.1016/j.jallcom.2015.03.172
16. C. Yuan, L. Zhang, L. Hou, L. Zhou, G. Pang, L. Lian, Scalable room-temperature synthesis of mesoporous nanocrystalline $ZnMn_2O_4$ with enhanced lithium storage properties for lithium-ion batteries. Chem. Eur. J. **21**(3), 1262–1268 (2015). doi:10.1002/chem.201404624
17. D. Cai, D. Wang, H. Huang, X. Duan, B. Liu, L. Wang, Y. Liu, Q. Li, T. Wang, Rational synthesis of $ZnMn_2O_4$ porous spheres and graphene nanocomposite with enhanced performance for lithium-ion batteries. J. Mater. Chem. A **3**(21), 11430–11436 (2015). doi:10.1039/C5TA00539F
18. Y. Sun, X. Hu, W. Luo, F. Xia, Y. Huang, Reconstruction of conformal nanoscale MnO on graphene as a high-capacity and long-life anode material for lithium ion batteries. Adv. Funct. Mater. **23**(19), 2436–2444 (2013). doi:10.1002/adfm.201202623
19. H. Xia, D. Zhu, Y. Fu, X. Wang, $CoFe_2O_4$-graphene nanocomposite as a high-capacity anode material for lithium-ion batteries. Electrochimi. Acta **3**, 166–174 (2012). doi:10.1016/j.electacta.2012.08.027
20. Y.S. Yang, C.Y. Wang, M.M. Chen, Z.Q. Shi, J.M. Zheng, Facile synthesis of mesophase pitch/exfoliated graphite nanoplatelets nanocomposite and its application as anode materials for lithium-ion batteries. J. Solid State Chem. **183**(9), 2116–2120 (2010). doi:10.1016/j.jssc.2010.07.011
21. C. Ma, C. Ma, J. Wang, H. Wang, J. Shi, Y. Song, Q. Guo, L. Liu, Exfoliated graphite as a flexible and conductive support for Si-based Li-ion battery anodes. Carbon **72**, 38–46 (2014). doi:10.1016/j.carbon.2014.01.027
22. Y.X. Wang, L. Huang, L.C. Sun, S.Y. Xie, G.L. Xu et al., Facile synthesis of a interleaved expanded graphite-embedded sulphur nanocomposite as cathode of Li–S batteries with excellent lithium storage performance. J. Mater. Chem. **22**(11), 4744–4750 (2012). doi:10.1039/c2jm15041g
23. Y. Zhao, C. Ma, Y. Li, H. Chen, Z. Shao, Self-adhesive Co_3O_4/expanded graphite paper as high-performance flexible anode for Li-ion batteries. Carbon **95**, 494–496 (2015). doi:10.1016/j.carbon.2015.08.053
24. D. Zhao, L. Wang, P. Yu, L. Zhao, C. Tian, W. Zhou, L. Zhang, H. Fu, From graphite to porous graphene-like nanosheets for high rate lithium-ion batteries. Nano Res. **8**(9), 2998–3010 (2015). doi:10.1007/s12274-015-0805-z
25. Y. Zhao, C. Ma, C. Ma, J. Shi, J. Shi, Facile solution-free preparation of a carbon coated Fe_3O_4 nanoparticles/expanded graphite composite with outstanding Li-storage performances. Mater. Lett. **177**, 148–151 (2016). doi:10.1016/j.matlet.2016.04.049
26. Y. Xiao, J. Zai, X. Li, Y. Gong, B. Li, Q. Han, X. Qian, Polydopamine functionalized graphene/$NiFe_2O_4$ nanocomposite with improving Li storage performances. Nano Energy **6**, 51–58 (2014). doi:10.1016/j.nanoen.2014.03.006
27. J. Zhu, T. Zhu, X. Zhou, Y. Zhang, X.W. Lou, X. Chen, H. Zhang, H.H. Hng, Q. Yan, Facile synthesis of metal oxide/reduced graphene oxide hybrids with high lithium storage capacity and stable cyclability. Nanoscale **3**(3), 1084–1089 (2011). doi:10.1039/C0NR00744G
28. G. Zhou, J. Ma, L. Chen, Selective carbon coating techniques for improving electrochemical properties of NiO nanosheets. Electrochim. Acta **133**, 93–99 (2014). doi:10.1016/j.electacta.2014.03.161
29. Y. Zhao, Z. Feng, Z.J. Xu, Yolk-shell Fe_2O_3 odot C composites anchored on MWNTs with enhanced lithium and sodium storage. Nanoscale **7**(21), 9520–9525 (2015). doi:10.1039/C5NR01281C
30. Z. Li, H. Wang, Z. Sun, J. Su, Z. Wang, L. Wang, Self-activated continuous pulverization film: an insight into the mechanism of the extraordinary long-life cyclability of hexagonal H4.5Mo5.25O18·(H2O)1.36 microrods. J. Mater. Chem. A **4**(1), 303–313 (2016). doi:10.1039/C5TA07314F
31. Y. Xiao, X. Li, J. Zai, K. Wang, Y. Gong, B. Li, Q. Han, X. Qian, $CoFe_2O_4$-graphene nanocomposites synthesized through an ultrasonic method with enhanced performances as anode materials for Li-ion batteries. Nano-Micro Lett. **6**(4), 307–315 (2014). doi:10.1007/s40820-014-0003-7
32. S. Yang, H. Song, X. Chen, Electrochemical performance of expanded mesocarbon microbeads as anode material for lithium-ion batteries. Electrochem. Commun. **8**(1), 137–142 (2006). doi:10.1016/j.elecom.2005.10.035
33. Y. Fu, Y. Wan, H. Xia, X. Wang, Nickel ferrite–graphene heteroarchitectures: toward high-performance anode materials for lithium-ion batteries. J. Power Sources **213**, 338–342 (2012). doi:10.1016/j.jpowsour.2012.04.039

34. B. Tian, J. Swiatowska, V. Maurice, S. Zanna, A. Seyeux, L.H. Klein, P. Marcus, Aging-induced chemical and morphological modifications of thin film iron oxide electrodes for lithium-ion batteries. Langmuir **30**(12), 3538–3547 (2014). doi:10.1021/la404525v
35. G. Wang, X. Shen, J. Yao, J. Park, Graphene nanosheets for enhanced lithium storage in lithium ion batteries. Carbon **47**, 2049–2053 (2009). doi:10.1016/j.carbon.2009.03.053
36. Y. Wu, Y. Wei, J. Wang, K. Jiang, S. Fan, Conformal Fe_3O_4 sheath on aligned carbon nanotube scaffolds as high-performance anodes for lithium ion batteries. Nano Lett. **13**(2), 818–823 (2013). doi:10.1021/nl3046409
37. G. Zhou, D.W. Wang, F. Li, L. Zhang, N. Li, Z.S. Wu, L. Wen, G.Q. Lu, H.M. Cheng, Graphene-wrapped Fe_3O_4 anode material with improved reversible capacity and cyclic stability for lithium ion batteries. Chem. Mater. **22**(18), 5306–5313 (2010). doi:10.1021/cm101532x
38. P. Zhu, S. Liu, J. Xie, S. Zhang, G. Cao, X. Zhao, Facile synthesis of $NiFe_2O_4$/reduced graphene oxide hybrid with enhanced electrochemical lithium storage performance. J. Mater. Sci. Technol. **30**(11), 1078–1083 (2014). doi:10.1016/j.jmst.2014.08.009
39. L. Wu, Q. Xiao, Z. Li, G. Lei, P. Zhang, L. Wang, $CoFe_2O_4$/C composite fibers as anode materials for lithium-ion batteries with stable and high electrochemical performance. Solid State Ionics **215**, 24–28 (2012). doi:10.1016/j.ssi.2012.03.044
40. L. Tao, J. Zai, K. Wang, Y. Wan, H. Zhang, C. Yu, Y. Xiao, X. Qian, 3D-hierarchical NiO-graphene nanosheet composites as anodes for lithium ion batteries with improved reversible capacity and cycle stability. RSC Adv. **2**(8), 3410–3415 (2012). doi:10.1039/c2ra00963c
41. S. Laruelle, S. Grugeon, P. Poizot, M. Dolle, L. Dupont, J. Tarascon, on the origin of the extra electrochemical capacity displayed by MO/Li cells at low potential. J. Electrochem. Soc. **149**(5), A627–A634 (2002). doi:10.1149/1.1467947
42. P. Preetham, S. Mohapatra, S. Nair, D. Santhanagopalan, A.K. Rai, Ultrafast pyro-synthesis of $NiFe_2O_4$ nanoparticles within a full carbon network as a high-rate and cycle-stable anode material for lithium ion. RCS Adv. **6**(44), 38064–38070 (2016). doi:10.1039/c6ra03670h
43. J. Wang, G. Yang, L. Wang, W. Yan, Synthesis of one-dimensional $NiFe_2O_4$ nanostructures: tunable morphology and high-performance anode materials for Li ion batteries. J. Mater. Chem. A **4**(22), 8620–8629 (2016). doi:10.1039/C6TA02655A
44. T. Wei, F. Wang, J. Yan, J. Cheng, Z. Fan, H. Song, Microspheres composed of multilayer graphene as anode material for lithium-ion batteries. J. Electroanaly. Chem. **653**(1–2), 45–49 (2011). doi:10.1016/j.jelechem.2011.01.010
45. C.M. Chen, J.Q. Huang, Q. Zhang, W.Z. Gong, Q.H. Yang, M. Wang, Y. Yang, Annealing a graphene oxide film to produce a free standing high conductive graphene film. Cabon **50**(2), 659–667 (2012). doi:10.1016/j.carbon.2011.09.022
46. L. Bai, D. Zhao, T. Zhang, W. Xie, J. Zhang, A comparative study of electrochemical performance of graphene sheets, expanded graphite and natural graphite as anode materials for lithium-ion batteries. Electrochim. Acta **107**, 555–561 (2013). doi:10.1016/j.electacta.2013.06.032